Decoherence and relaxation of single electron excitations in quantum Hall edge channels.

Pascal Degiovanni, Charles Grenier, Gwendal Fève

Decoherence and relaxation of single electron excitations in quantum Hall edge channels.

P. Degiovanni[1], Ch. Grenier[1], and G. Fève[2]
(1) Université de Lyon, Fédération de Physique André Marie Ampère,
CNRS - Laboratoire de Physique de l'Ecole Normale Supérieure de Lyon,
46 Allée d'Italie, 69364 Lyon Cedex 07, France and
(2) Laboratoire Pierre Aigrain, Département de Physique de l'Ecole Normale Supérieure,
24 rue Lhomond, 75231 Paris Cedex 05, France

A unified approach to decoherence and relaxation of energy resolved single electron excitations in Integer Quantum Hall edge channels is presented. Within the bosonization framework, relaxation and decoherence induced by interactions and capacitive coupling to an external linear circuit are computed. An explicit connexion with high frequency transport properties of a two terminal device formed by the edge channel on one side and the linear circuit on the other side is established.

PACS numbers: 73.23.-b,03.65.Yz,73.43.Cd,73.43.Lp

Electronic transport along the edges of a 2DEG in the Integer Quantum Hall regime has given rise to a strong experimental and theoretical work during last decades. Along these chiral edge channels, electronic propagation is ballistic and phase coherent over tens of microns. Consequently, strong analogies with photon propagation have been pointed out: for example, electrons are guided along edge channels which, at first sight, play the role of optical fibers. Moreover quantum point contacts can be considered as electronic beamsplitters of adjustable transmission. These analogies have been best illustrated by the demonstration of electronic Mach-Zehnder interferometers [1, 2, 3]. Recently, the development of an on demand single electron source [4] that emits a single electron in a chiral edge opens the way to fundamental quantum optics experiments involving single charge excitations. Typical examples are the electronic Hanbury-Brown and Twiss experiment [5] or the Hong-Ou-Mandel experiment [6] in which two indistinguishable electrons collide on the beam-splitter.

But contrary to photons, electrons interact with their electromagnetic environment and with other electrons present the Fermi sea. This results in relaxation and decoherence of single electron excitations above the ground state. Such differences have been emphasized in Mach-Zehnder interferometers where, despite insensitivity to electron-source time coherence, decoherence along the chiral edges drastically reduces the contrast of interferences [7, 8, 9, 10, 11, 12]. Recently, energy resolved electronic detection using quantum dots has also been demonstrated [13], thus opening the way to energy relaxation studies in quantum Hall edge channels. A full development of electron quantum optics thus requires a comprehensive understanding of these effects.

In this letter, we present a unified approach of high frequency transport and decoherence and relaxation of coherent single electron excitations in quantum Hall edge channels. Within the bosonization framework, electronic transport is equivalently described by the propagation of charge density waves called plasmons. Electron interactions within the edge channel or with an external environment results in the scattering of plasmons and possibly involved environmental modes. We show that plasmon scattering can be mapped onto the high frequency admittance of the two-terminal device including the chiral edge on one side and its environment on the other (see Fig. 1-a). Applying quantum optics concepts to plasmons, we finally show that it also determines relaxation and decoherence of coherent single electron excitations.

Model Let us consider the specific example of a chiral edge channel capacitively coupled to an external gate of size l connected to a resistance R representing a dissipative external circuit (see Fig. 1). In the integer quantum Hall regime, bosonization expresses the electron creation operator at point x along the edge, $\psi^\dagger(x)$, in terms of a chiral bosonic field $\phi(x)$ as:

$$\psi^\dagger(x) = \frac{U^\dagger}{\sqrt{2\pi a}} e^{-i\sqrt{4\pi}\phi(x)}, \tag{1}$$

where a is a short distance cutoff and $U^\dagger$ ensures fermionic anticommutation relations. The bosonic field determines the electron density $n(x) = (\partial_x \phi)(x)/\sqrt{\pi}$. In the presence of an external voltage $U(x,t)$ along the edge, its equation of motion is:

$$(\partial_t + v_F \partial_x)\, \phi(x,t) = \frac{e\sqrt{\pi}}{h}\, U(x,t)\,. \tag{2}$$

where v_F is the electron Fermi velocity along the edge. Before and after the interaction region $|x| \leq l/2$, this chiral field propagates freely and thus defines input ($j = \text{in}$ for $x \leq -l/2$) and output ($j = \text{out}$ for $x \geq l/2$) plasmon modes :

$$\phi_j(x,t) = \frac{-i}{\sqrt{4\pi}} \int_0^\infty \frac{d\omega}{\sqrt{\omega}} (b_j(\omega) e^{i\omega(x/v_F - t)} - \text{h.c})\,. \tag{3}$$

In the interaction area $|x| \leq l/2$, the edge is capacitively coupled to the gate forming a capacitor of capacitance C. Following Büttiker *et al.* [14], we assume the potential within the edge to be uniform [22] and denoted by $U(t)$ [14]. The total charge stored within the interaction region

$$Q(t) = -e\int_{-l/2}^{l/2} n(x,t)\,dx \qquad (4)$$

is proportional to the voltage drop between the gate at potential $V(t)$ and the edge channel:

$$C(U(t)-V(t)) = Q(t)\,. \qquad (5)$$

Following [15, 16], the resistance will be modeled as a quantum transmission line with characteristic impedance $Z=R$. Its degrees of freedom are described by input and output photon modes $a_j(\omega)$ ($j=$ in or out) propagating along the line. The total charge stored within the line is, by neutrality of the RC circuit, equal to $Q(t)$ and expressed in terms of photon modes by:

$$Q(t) = \sqrt{\frac{\hbar}{4\pi R}}\int_0^\infty ((a_{\mathrm{in}}+a_{\mathrm{out}})(\omega)e^{-i\omega t}+\mathrm{h.c.})\frac{d\omega}{\sqrt{\omega}}\,. \qquad (6)$$

The voltage of the gate $V(t)$ is also expressed as:

$$V(t) = eR\sqrt{\frac{R_K}{2R}}\int_0^\infty \sqrt{\omega}(i(a_{\mathrm{in}}-a_{\mathrm{out}})(\omega)e^{-i\omega t}+\mathrm{h.c.})\frac{d\omega}{2\pi} \qquad (7)$$

Using (5), (6) and (7), the voltage $U(t)$ can be expressed in terms of the a modes. Solving for the edge equation of motion (2) gives a first linear equation relating the input and output a and b modes. It also expresses the chiral field and total charge within the interaction region in terms of these modes. Using this in eq. (4) leads to a second linear equation between the input and output a and b modes. From these two linear equations, the unitary plasmon to photon scattering matrix $S(\omega)=(S_{\alpha\beta}(\omega))$ (α, β equal to c for the circuit or e for the edge) at frequency $\omega/2\pi$ can be extracted. In the following $t(\omega)=S_{ee}(\omega)$ will denote the edge plasmon transmission amplitude. We now show that it determines both the finite frequency admittance and single electron relaxation.

High frequency admittances The admittance matrix at frequency ω relates the Fourier component $I_\alpha(\omega)$ of the incoming currents through the various leads α to the voltages $V_\beta(\omega)$ in the linear response regime:

$$I_\alpha(\omega) = \sum_\beta g_{\alpha\beta}(\omega)\,V_\beta(\omega)\,. \qquad (8)$$

In the present case, the input modes can be related to the voltages applied to the edge reservoir and to the RC circuit. First of all, the applied time dependent voltage $V_c(t)$ creates an incoming coherent state within the transmission line caracterized by the average value of the incoming a modes:

$$\langle a_{\mathrm{in}}(\omega)\rangle = \frac{-i}{\sqrt{\omega}}\sqrt{\frac{R_K}{2R}}\frac{eV_c(\omega)}{h}\,. \qquad (9)$$

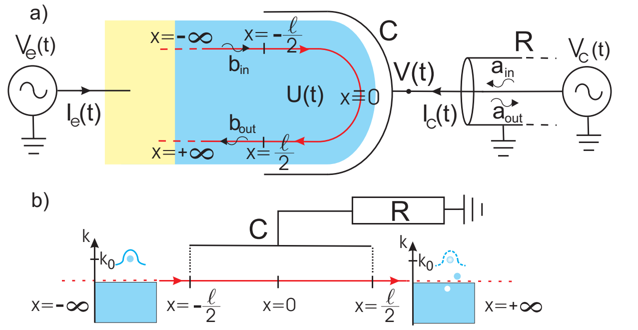

FIG. 1: (Color) (a) Two terminal device built from an edge channel coupled to an RC circuit. In the interaction area $|x|\leq l/2$, the edge channel (in red) at internal potential $U(t)$ is capacitively coupled to the gate of capacitance C at potential $V(t)$. (b) A single electron is injected in the $x<-l/2$ region and propagates along the edge channel. Interactions within $|x|\leq l/2$ create electron/hole pairs within the edge channel and photons in the RC circuit leading to decoherence.

For the edge channel, modeling the reservoir as a uniform time dependent voltage $V_e(t)$ applied from $x=-\infty$ to $x=-l/2$ shows that it injects in the $[-l/2,l/2]$ region a plasmon coherent state fully characterized by the average value of the incoming b modes [17]:

$$\langle b_{\mathrm{in}}(\omega)\rangle = -\frac{e}{h}\frac{V_e(\omega)}{\sqrt{\omega}}\,e^{i\omega l/2v_F}\,. \qquad (10)$$

The finite frequency admittance can then be expressed in terms of the plasmon to photon scattering matrix and reciprocally uniquely determines it. In the present case, due to total screening of charges in the edge channel by the gate, this 2×2 admittance matrix satisfies gauge invariance and charge conservation [14]: $g_{ee}=g_{cc}=-g_{ec}=-g_{ce}$ and is thus determined by a unique admittance :

$$g(\omega) = g_{ee}(\omega) = \frac{e^2}{h}(1-t(\omega)\,e^{i\omega v_F/l}), \qquad (11)$$

which is in turn entirely determined by the plasmon transmission amplitude $t(\omega)$. At low frequency and up to second order in ω, the admittance is equivalent to the serial addition of a electrochemical capacitance C_μ and a charge relaxation resistance R_q. Here, C_μ is the series addition of the quantum capacitance $C_q=l/v_FR_K$ (with $R_K=\frac{h}{e^2}$) and the geometric capacitance [14]. The charge relaxation resistance is the sum of the circuit resistance and the half-quantum $h/2e^2$ [18, 19] expected for a single mode conductor.

Electron relaxation and decoherence Let us now consider the evolution of a single electron initially prepared (see Fig. 1-b) in a coherent wave packet. Starting from the zero temperature [23] Fermi sea $|F\rangle$, the many body state with one additional electron in the normalized wavepacket $\varphi(x)$ above the Fermi sea is given by $|\varphi,F\rangle = \int\varphi(x)\psi^\dagger(x)|F\rangle\,dx$.

Single particle spatial coherence and density are respectively described by the off diagonal and diagonal components of the single particle reduced density operator $\mathcal{G}_\rho^{(e)}(x,y) = \mathrm{Tr}(\psi(x).\,\rho.\,\psi^\dagger(y))$ in which ρ denotes the many body electronic density operator. Going to Fourier space then shows that the single electron momentum distribution is encoded in the diagonal of the single particle density operator in momentum space.

Before entering the interaction region, the initial many body density operator is given by $\rho_i = |\varphi, F\rangle\langle\varphi, F|$ and then $\mathcal{G}_{\rho_i}^{(e)}(x,y) = \mathcal{G}_F^{(e)}(x,y) + \varphi(y)^*\varphi(x)$ where the first contribution $\mathcal{G}_F^{(e)}(x,y) = \int n_F(k) e^{ik(x-y)} \frac{dk}{2\pi}$ comes from the Fermi sea ($n_F(k) = \langle c_k^\dagger c_k\rangle_F$) whereas the second one is associated with the coherent single electron excitation.

Using (1), the state $|\varphi, F\rangle$ appears as a superposition of incoming plasmon coherent states. Since the interaction region elastically scatters plasmon to photons, the resulting outcoming external circuit + edge quantum state is an entangled superposition of coherent plasmon and photon states. Tracing out over the circuit's degrees of freedom leads to the exact many body electron state after time t such that the initial wave packet has flown through the interacting region:

$$\begin{aligned}\rho_f &= \int dy_+ dy_- \varphi(y_+)\varphi^*(y_-)\mathcal{D}_{\mathrm{ext}}(y_+ - y_-) \\ &\times\ \widetilde{\psi}^\dagger(y_+ + v_F t)|F\rangle\langle F|\widetilde{\psi}(y_- + v_F t) \qquad (12)\end{aligned}$$

where $\mathcal{D}_{\mathrm{ext}}$ is the extrinsic decoherence associated with photon emission into the external circuit

$$\mathcal{D}_{\mathrm{ext}}(\Delta y) = \exp\left(\int_0^{+\infty} |r(\omega)|^2 \,(e^{-i\frac{\omega\,\Delta y}{v_F}} - 1)\,\frac{d\omega}{\omega}\right) \quad (13)$$

where $r(\omega) = S_{ce}(\omega)$ denotes the plasmon to photon scattering amplitude. In (12), $\widetilde{\psi}^\dagger(y)$ is a modified field operator:

$$\widetilde{\psi}^\dagger(y) = \frac{U^\dagger}{\sqrt{2\pi a}} \exp\left(\int_0^\infty (t(\omega) b(\omega)\, e^{i\omega y/v_F} - \mathrm{h.c.}) \frac{d\omega}{\sqrt{\omega}}\right). \quad (14)$$

When $t(\omega)$ is a pure phase linear in ω, $\widetilde{\psi}^\dagger(y)$ is a spatially translated fermion field operator. Any other ω dependence of $t(\omega)$ leads to the creation of additional electron/hole pairs that cannot be absorbed in a simple translation.

Relaxation of a single electron can then be discussed by considering an incident energy resolved wave function: $\varphi_{k_0}(x) = e^{ik_0 x}$. The complete momentum distribution consists in the Fermi sea contribution and a change $\delta n(k,k_0)$ that can be obtained from single particle coherence $\mathcal{G}_{k_0}^{(e)}$ after interaction with the RC-circuit:

$$\int_{\mathbb{R}} e^{-ik(x-y)} \mathcal{G}_{k_0}^{(e)}(x,y)\, d(x-y) = L n_F(k) + \delta n(k,k_0) \quad (15)$$

where L is the total size of the system. The l.h.s. can be computed using bosonization thus leading to explicit fully non perturbative expressions for single electron relaxation $\delta n(k,k_0)$ that will be given in a forthcoming publication.

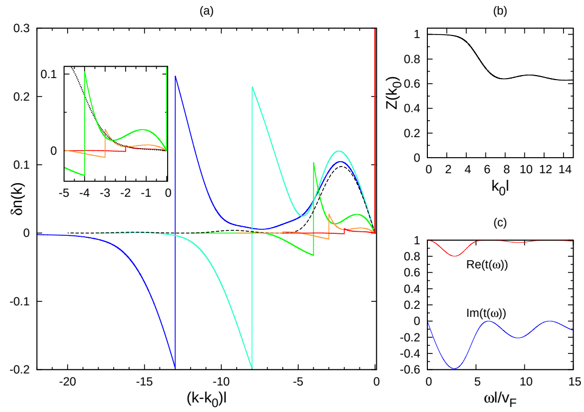

FIG. 2: (Color) (a) Single electron energy relaxation for $R = 50\ \Omega$ and $l/v_F R_K C = 0.5$ plotted against $(k-k_0)l$ for $k_0 l = 2$ (red), 3 (orange), 4 (green), 8 (cyan) and 13 (purple). The dashed curve corresponds to the single particle result (16) valid at high energies. Inset shows the zoom for small kl. The dotted line corresponds to the simple relaxation model $\delta n_r(k,k_0) = -Z'(k_0 - k)$. (b) Quasiparticle peak $Z(k_0)$. (c) Real and imaginary part of the plasmon transmission amplitude $t(\omega)$.

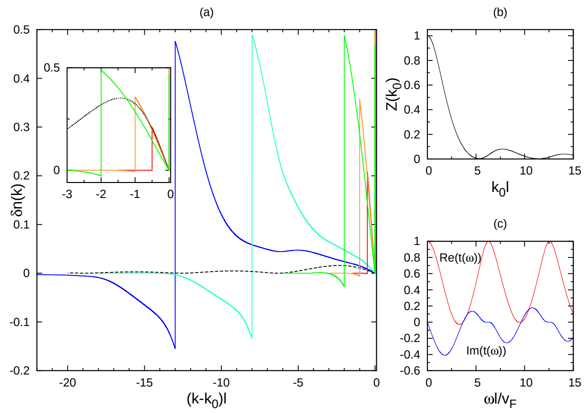

FIG. 3: (Color) (a) Single electron energy relaxation for $R/R_K = 0.5$ and $l/v_F R_K C = 0.5$ plotted against $(k-k_0)l$ for $k_0 l = 0.5$ (red), 1 (orange), 2 (green), 8 (cyan) and 13 (purple). The dashed curve corresponds to the single particle result (16) valid at high energies. Inset shows the zoom for small kl. The dotted line corresponds to the simple relaxation model $\delta n_r(k,k_0) = -Z'(k_0 - k)$. (b) Quasiparticle peak $Z(k_0)$. (c) Real and imaginary part of the plasmon transmission amplitude $t(\omega)$.

This detailed analysis shows that, at zero temperature, $\delta n(k,k_0)$ has a quasiparticle peak at $k = k_0$ and a non-zero regular part for $-k_0 \leq k < k_0$: $\delta n(k,k_0) = Z(k_0)\delta(k-k_0) + \delta n_r(k,k_0)$. It can be shown that the remaining quasi-particle weight $Z(k_0)$ is the square modulus of the amplitude appearing in the reduction of the fringe contrast for single electron excitations injected in the Mach-Zehnder interferometer [9, 10, 12]. Finally, the sum rule $Z(k_0) + \int_{-k_0}^{k_0} \delta n_r(k,k_0) dk = 1$ reflects particle conservation.

Fig. 2-a presents the regular part $\delta n_r(k,k_0)$ as a function of $(k-k_0)l$ at fixed k_0, and fig. 2-c shows the weight of the quasiparticle peak $Z(k_0)$ in term of $k_0 l$ for $R = 50\ \Omega$ and $l/v_F R_K C = 0.5$. In two limiting regimes, energy relaxation can be described using a single particle relaxation approach by introducing an appropriate effective environment and, at low energy, taking into account the Pauli exclusion principle.

Close enough to the Fermi surface (see inset fig. 2-a), single electron relaxation can be described using a simple relaxation model : for $0 \leq k < k_0$, $\delta n_r(k,k_0) \simeq p(k_0-k)$ where $p(q)$ can be interpreted as the probability to lose momentum q. The remaining quasiparticle weight $Z(k_0)$ is then related to p by $p(q) = -Z^{'}(q)$. Note that the Fermi sea remains spectator ($\delta n_r(k,k_0) \simeq 0$ for $k < 0$), since at low energies $t(\omega)$ is close to one, thus limiting the creation of electron/hole pairs in the relaxation process. In this regime, energy relaxation is limited by the Pauli exclusion principle. For $R \neq 0$ and at low energy, photon emission is the dominant relaxation mechanism and the inelastic scattering probability $1 - Z(k_0)$, which only depends on the equivalent circuit parameters, scales as $(\frac{R_q}{R_K} - \frac{1}{2})(k_0 R_K C_\mu/v_F)^2$ at low momentum. Consequently, the quasi particle is well defined close to the Fermi surface.

At high energies, $\delta n(k,k_0)$ splits into two distinct contributions (see *e.g* fig. 2-a, $k_0 l = 8,\ 13$). The first one appears in Fourier space around the Fermi level and corresponds to the electron/hole pairs created by the incident electron. The second one is localized in Fourier space close to k_0 and corresponds to the relaxation of the incoming electron due to photon emission into the transmission line as well as electron/hole pair creation inside the edge channel. In real space, in the limit of very high incident energy, it shows up as an effective decoherence coefficient $\mathcal{D}(x-y)$ acting on the incident wavepacket propagated during the time interval $[0,t]$:

$$\varphi(x)\varphi^*(y) \mapsto \varphi(x-v_F t)\varphi^*(y-v_F t)\,\mathcal{D}(x-y)\,. \quad (16)$$

The decoherence coefficient is then a product $\mathcal{D} = \mathcal{D}_{\text{ext}} \times \mathcal{D}_{\text{int}}$ of the extrinsic contribution (13) and an intrinsic contribution associated with the imprints left within the Fermi sea by the different positions appearing in the single electron incident wavepacket. Explicitly, provided $t(\omega)$ goes to 1 for $\omega \to +\infty$, $\mathcal{D}_{\text{int}}$ is obtained from (13) by replacing $r(\omega)$ by $1-t(\omega)$ to account for the e/h pairs contained in $\widetilde{\psi}^\dagger(y)|F\rangle$ compared to $\psi^\dagger(y)|F\rangle$. Finally $\mathcal{D}$ is obtained by substituting $|r(\omega)|^2$ by $2\Re(1-t(\omega))$ into (13). This regime is similar to the dynamical Coulomb blockade [20], with the Fourier transform of $\mathcal{D}$ playing the role of $P(E)$ (see dashed lines on figs. 2-a and 3-a for the corresponding energy relaxation). The case of an RC-circuit with $R = R_K/2$ exhibits clear deviations from these two limiting approaches in the considered frequency range (see fig. 3-a) thus showing the need of our non-perturbative approach. This arises from the strong plasmon scattering in the relevant frequency range at larger R/R_K (compare figs. 2-c and 3-c). Note also the faster decay of the quasiparticle peak (compare figs. 2-b and 3-b).

Conclusion In this letter, we have presented a complete theory of coherent single electron excitation relaxation in integer quantum Hall edge channels induced by capacitive coupling to a linear circuit. Within the bosonization framework, the scattering between edge plasmonic and environmental modes determines both the finite frequency admittances and relaxation properties of a coherent single electron excitation. The latter can thus be computed exactly from the finite frequency admittances. This approach can be used to study decoherence and relaxation of single electron excitations due to interactions within a single edge channel or to interchannel coupling in $\nu = 2$ quantum Hall systems. It can also be generalized to fractional quantum Hall edges as well as to the case of non chiral quantum wires. Finally, relaxation of non equilibrium distribution functions such as the one created by a biased quantum point contact requires taking into account all Keldysh correlators of currents [21].

Acknowledgments

We warmly thank Ch. Glattli, B. Plaçais, F. Pierre and P. Roche for useful discussions and remarks.

[1] Y. Ji, Y. Chung, D. Sprinzak, M. Heiblum, D. Mahalu, and H. Shtrikman, Nature **422**, 415 (2003).
[2] I. Neder, N. Ofek, Y. Chung, M. Heiblum, D. Mahalu, and V. Umansky, Nature **448**, 333 (2007).
[3] P. Roulleau, F. Portier, D.C. Glattli, P. Roche, A. Cavanna, G. Faini, U. Gennser, and D. Mailly, Phys. Rev. Lett. **100**, 126802 (2008).
[4] G. Fève, A. Mahé, J. Berroir, T. Kontos, B. Plaçais, D.C. Glattli, A. Cavanna, B. Etienne, and Y. Jin, Science **316**, 1169 (2007).
[5] R. Hanbury-Brown and R. Twiss, Nature **178**, 1046 (1956).
[6] C.K. Hong, Z.Y. Ou, and L. Mandel, Phys. Rev. Lett. **59**, 2044 (1987).
[7] J.T. Chalker, Y. Gefen, and M.Y. Veillette, Phys. Rev. **B 76**, 085320 (2007).
[8] P. Roulleau, F. Portier, P. Roche, A. Cavanna, G. Faini, U. Gennser, and D. Mailly, Phys. Rev. Lett. **101**, 186803 (2008).
[9] I.P. Levkivskyi and E.V. Sukhorukov, Phys. Rev. **B 78**, 045322 (2008).
[10] C. Neuenhahn and F. Marquardt, Phys. Rev. Lett. **102**,

046806 (2009).
[11] G. Seelig and M. Büttiker, Phys. Rev. **B 64**, 245313 (2001).
[12] E.V. Sukhorukov and V.V. Cheianov, Phys. Rev. Lett. **99**, 156801 (2007).
[13] C. Altimiras, H. le Sueur, U. Gennser, A. Cavanna, D. Mailly, and F. Pierre (2009), private communication.
[14] A. Prêtre, H. Thomas, and M. Büttiker, Phys. Rev. **B 54**, 8130 (1996).
[15] B. Yurke, and J.S. Denker, Phys. Rev. **A 29**, 1419 (1984).
[16] G. Fève, P. Degiovanni, and T. Jolicoeur, Phys. Rev. **B 77**, 035308 (2008).
[17] I. Safi, Eur. Phys. J. **D 12**, 451 (1999).
[18] M. Büttiker, H. Thomas, and A. Prêtre, Phys. Lett. A p. 364 (1993).
[19] J. Gabelli, G. Fève, J. Berroir, B. Plaçais, A. Cavanna, B. Etienne, Y. Jin, and D.C. Glattli, Science **313**, 5786 (2006).
[20] G.-L. Ingold and Y. Nazarov, *Single charge tunneling* (Plenum Press, New York, 1992), vol. 294 of *NATO ASI Series B*, chap. Charge tunneling rates in ultrasmall junctions, pp. 21–107.
[21] I. Snyman and Y.V. Nazarov, Phys. Rev. **B 77**, 165118 (2008).
[22] This hypothesis is valid for $\omega/2\pi \lesssim v_F/l$ but one should keep in mind that the general framework presented here is model independent and thus remains valid for more realistic models of circuit/edge channel coupling.
[23] This discussion can easily be generalized to finite temperature.